

## A HYBRID ANALYTICAL-NUMERICAL TECHNIQUE FOR ELLIPTIC PDES\*

MATTHEW J. COLBROOK<sup>†</sup>, THANASIS S. FOKAS<sup>†</sup>, AND PARHAM HASHEMZADEH<sup>†</sup>

**Abstract.** Recent work has given rise to a novel and simple numerical technique for solving elliptic boundary value problems formulated in convex polygons in two dimensions. The method, based on the unified transform, involves expanding the unknown boundary values in a Legendre basis and determining the expansion coefficients by evaluating the so-called global relation at appropriate points in the complex Fourier plane (spectral collocation). In this paper we provide a significant advancement of this numerical technique by providing a fast and efficient method to evaluate the solution in the domain interior. The use of a Legendre basis allows the relevant integrals to be computed efficiently and accurately using Chebyshev interpolation, even for large degree. For the particular case of the Laplace equation this allows an explicit expansion in the domain interior in terms of hypergeometric functions. Evaluation in the interior is found to converge more rapidly than the approximation of the unknown boundary values, allowing accurate approximation of solutions with weak corner singularities. For stronger singularities, the method can be combined with global singular functions for rapid convergence. Numerical examples are provided, showing that the method compares well against standard spectral methods and opens up the possibility of applying the method to general curvilinear domains.

**Key words.** uniform transform method, spectral methods, elliptic PDEs, boundary value problems

**AMS subject classifications.** 65N35, 65N12, 35J25

**DOI.** 10.1137/18M1217309

**1. Introduction.** The *unified transform* [27, 28, 29] is a method for analyzing boundary value problems (BVPs) for linear PDEs with constant coefficients [25, 60, 44], as well as for integrable nonlinear PDEs [48, 30]. A crucial role in the method is played by the so-called *global relation* formulated in the complex Fourier plane, which is an algebraic equation coupling appropriate integral transforms of all boundary values. This relation has had important analytical and numerical implications: first, it provides the starting point for placing the implementation of the unified transform to elliptic PDEs on a rigorous foundation [5]. Second, it has led to novel analytical formulations of a variety of important physical problems from water waves [1, 23, 8, 46, 61, 24] to three-dimensional layer scattering [3]. Third, it has led to the emergence of a new, now established, numerical technique for the Laplace, modified Helmholtz, Helmholtz, and biharmonic equations on convex domains in two dimensions [31, 21, 35, 34, 51, 52, 53, 54, 55, 6, 33, 16]. Namely, the analysis of the global relation gives rise to a simple algorithm for the numerical computation of the *generalized Dirichlet-to-Neumann map*, i.e., for determining the unknown boundary values in terms of the given boundary data.

---

\*Submitted to the journal's Methods and Algorithms for Scientific Computing section October 9, 2018; accepted for publication (in revised form) February 11, 2019; published electronically April 9, 2019.

<http://www.siam.org/journals/sisc/41-2/M121730.html>

**Funding:** This work was supported by EPSRC grant EP/L016516/1 for the University of Cambridge Centre for Analysis.

<sup>†</sup>Department of Applied Mathematics and Theoretical Physics, University of Cambridge, Cambridge, CB3 0WA, United Kingdom (m.colbrook@damtp.cam.ac.uk, tf227@cam.ac.uk, ph442@cam.ac.uk).

The latter technique provides an interesting collocation method, with collocation occurring in Fourier space rather than physical space. However, despite the many works on the method in the literature, there still remains much to be done in overcoming obstacles and assessing its scope. In particular, so far this method has been mainly used for computing the unknown boundary values, and there is very little discussion in the literature on how to effectively use this method to compute solutions in the interior. In many problems, such as the determination of the far-field pattern in scattering problems, computing boundary values of solutions to elliptic PDEs is sufficient to reveal quantities of interest. However, in a variety of problems, such as in plasmonics (regarding the precise field enhancements in a neighborhood of layer interfaces) it is necessary to compute the solution inside the domain. In this paper we show that the unified transform is effective for obtaining the solution of the BVP in the interior of the domain of interest, while still retaining the advantages of being a “boundary-based” method. We propose a fast and accurate numerical method employing the computed boundary values to evaluate the solution in the domain interior. Importantly, our analysis also allows the numerical treatment of domains whose boundary consists of a finite number of  $C^1$  curved edges.

We shall focus on the following linear PDE problem posed on a bounded Lipschitz domain  $\Omega$  with sides  $\Gamma_j$  listed in positive orientation:

$$(1.1) \quad \begin{aligned} &u_{xx} + u_{yy} \pm \kappa^2 u = 0 \text{ in } \Omega, \\ &\delta_j \frac{\partial u_j}{\partial \mathcal{N}} + (1 - \delta_j) u_j = g_j \quad \text{on } \Gamma_j, \quad j = 1, \dots, n. \end{aligned}$$

We take  $\kappa \in \mathbb{R}_{\geq 0}$  with  $\kappa = 0$  corresponding to the Laplace equation,  $+\kappa^2$  the Helmholtz equation, and  $-\kappa^2$  the modified Helmholtz equation. By a linear change of variables, our results can be extended to more general constant coefficient second order elliptic PDEs. For a side  $\Gamma_j$  we consider either a Dirichlet boundary condition ( $\delta_j = 1$ ) or a Neumann boundary condition ( $\delta_j = 0$ ). Such a problem is well-posed given sufficiently smooth boundary data and provided  $\mp \kappa^2$  is not an eigenvalue of the Laplacian on  $\Omega$  with the given boundary conditions [43].

The unified transform solves this BVP by employing the global relation, which provides a linear relationship between the known boundary data and the unknown boundary values. Specifically, if the domain is a polygon characterized by the corners  $z_j = x_j + iy_j$ ,  $z_j \in \mathbb{C}$ ,  $j = 1, \dots, n$ , then the global relation is given by

$$(1.2) \quad \sum_{j=1}^n \hat{u}_j(\lambda) = 0, \quad \lambda \in \mathbb{C},$$

where the function  $\hat{u}_j(\lambda)$  is the following Fourier transform along the side  $(z_j, z_{j+1})$ :

$$(1.3) \quad \hat{u}_j(\lambda) = \int_{z_j}^{z_{j+1}} e^{-i\lambda z} \left[ \frac{\partial u_j}{\partial \mathcal{N}} \frac{ds}{dz} + \lambda u_j \right] dz \quad \lambda \in \mathbb{C} \quad (\text{Lap.}),$$

$$(1.4) \quad \hat{u}_j(\lambda) = \int_{z_j}^{z_{j+1}} e^{\frac{i\kappa}{2}(\bar{z} - \lambda z)} \left[ \frac{\partial u_j}{\partial \mathcal{N}} \frac{ds}{dz} + \frac{\kappa u_j}{2} \left( \lambda + \frac{1}{\lambda} \frac{d\bar{z}}{dz} \right) \right] dz \quad \lambda \in \mathbb{C} \setminus \{0\} \quad (\text{mod. Helm.}),$$

$$(1.5) \quad \hat{u}_j(\lambda) = \int_{z_j}^{z_{j+1}} e^{\frac{-i\kappa}{2}(\lambda z + \bar{z})} \left[ \frac{\partial u_j}{\partial \mathcal{N}} \frac{ds}{dz} + \frac{\kappa u_j}{2} \left( \lambda - \frac{1}{\lambda} \frac{d\bar{z}}{dz} \right) \right] dz \quad \lambda \in \mathbb{C} \setminus \{0\} \quad (\text{Helm.}).$$

Here and throughout the paper  $\frac{\partial u_j}{\partial \mathcal{N}}$  denotes the derivative of  $u$  in the direction of the outward normal to the side  $(z_j, z_{j+1})$ , and  $s$  denotes the arc length parametrizing this side. These relations are a simple consequence of applying Green’s second identity to solutions of the adjoint equation (see, for example, [35]).

**The unified transform as a numerical algorithm.** For the benefit of the reader, we briefly recall how the global relation (1.2) gives rise to a collocation method for the case of a polygonal domain. Using the fact that  $\lambda$  is an arbitrary complex parameter, the analysis of the global relation yields a unique solution [5, 9, 7] for the unknown boundary values. This solution can be obtained numerically using the following steps:

- (i) Parametrize the  $j$ th side of the polygon, which is the side between the edges  $z_j$  and  $z_{j+1}$ , via the expressions

$$(1.6) \quad z(t) = m_j + th_j, \quad m_j = \frac{z_j + z_{j+1}}{2}, \quad h_j = \frac{z_{j+1} - z_j}{2}, \quad t \in [-1, 1].$$

- (ii) Expand  $\{u_j\}_1^n$  and  $\{\frac{\partial u_j}{\partial \mathcal{N}}\}_1^n$  in terms of  $N \in \mathbb{N}$  Legendre polynomials,<sup>1</sup>

$$(1.7) \quad u_j(t) \approx \sum_{l=0}^{N-1} a_l^j P_l(t), \quad \frac{\partial u_j}{\partial \mathcal{N}}(t) \approx \sum_{l=0}^{N-1} b_l^j P_l(t), \quad j = 1, \dots, n, \quad t \in [-1, 1].$$

For Dirichlet, Neumann, or Robin ( $\delta_j \neq 0, 1$ ) BVPs, a linear relation between  $a_l^j$  and  $b_l^j$  is known for each  $j$ .

- (iii) Substitute (1.7) into the global relation to obtain an *approximate global relation*. The approximate global relation is given by

$$(1.8) \quad \sum_{j=1}^n \hat{u}_j(\lambda) \approx 0 \quad \lambda \in \mathbb{C},$$

where for the Laplace equation,  $\hat{u}_j(\lambda)$  is obtained by substituting (1.7) into (1.3):

$$(1.9) \quad \hat{u}_j(\lambda) \approx \sum_{l=0}^{N-1} e^{-im_j \lambda} \left( b_l^j |h_j| + a_l^j h_j \lambda \right) \hat{P}_l(h_j \lambda) \quad \lambda \in \mathbb{C},$$

with  $\hat{P}_l(\lambda)$  denoting the finite Fourier transform of the Legendre polynomials:

$$(1.10) \quad \hat{P}_l(\lambda) = \int_{-1}^1 e^{-i\lambda t} P_l(t) dt = \frac{\sqrt{-2\pi i \lambda}}{-i\lambda} I_{l+1/2}(-i\lambda), \quad l = 0, \dots, N-1 \quad \lambda \in \mathbb{C},$$

where  $I_\alpha$  denotes the modified Bessel function of the first kind. Similar relations hold for the Helmholtz and modified Helmholtz equations.

---

<sup>1</sup>Legendre polynomials are used here because they satisfy the relation (1.10). In the literature of the unified transform, Legendre polynomials are found to be more accurate/stable than other choices, such as Chebyshev polynomials. Furthermore, the method we propose here makes vital use of the orthogonality of Legendre polynomials.

- (iv) Evaluate (1.8), as well as the Schwartz conjugate of (1.8), i.e., the equation obtained from (1.8) by taking its complex conjugate and then replacing  $\bar{\lambda}$  with  $\lambda$ , at an appropriate set of points (collocation points), and then compute a least-squares solution of the resulting system of linear equations for the unknown expansion coefficients. A suitable choice for collocation points is given in [35], and it is repeated below for completeness:

$$(1.11) \quad \lambda_{j,r} = -\bar{h}_j \frac{R}{M} r, \quad j = 1, \dots, n, \quad r = 1, \dots, M,$$

where the positive integer  $M$  specifies the total number of collocation points and the positive number  $R$  specifies the distance between consecutive collocation points. The above particular choice of collocation points has the advantage that it yields a linear algebraic system for the expansion coefficients  $\{a_l^j, b_l^j\}$  which has a low condition number. For a different numerical approach tackling several well-studied Wiener–Hopf problems for harmonic and biharmonic fields we refer the reader to [20]. This approach instead requires analysis of the zeros of functions arising from the global relations.

**Contribution of the paper.** The main contributions/novelties of the paper are the following:

- We demonstrate that after the unknown coefficients appearing in the Legendre expansions have been determined by the above algorithm, it is straightforward to compute the solution at any point  $z$  inside the domain. Indeed, let  $G$  be the associated fundamental solution of (1.1); then

$$(1.12) \quad u(x, y) = \int_{\partial\Omega} \left( G(x, y; \xi(s), \eta(s)) \frac{\partial u}{\partial \mathcal{N}} - u \frac{\partial G}{\partial \mathcal{N}}(x, y; \xi(s), \eta(s)) \right) ds.$$

Introducing the variable  $\zeta = \xi + i\eta$ , the chain rule yields the relations

$$(1.13) \quad \frac{\partial}{\partial \eta} = i \left( \frac{\partial}{\partial \zeta} - \frac{\partial}{\partial \bar{\zeta}} \right), \quad \frac{\partial}{\partial \xi} = \left( \frac{\partial}{\partial \zeta} + \frac{\partial}{\partial \bar{\zeta}} \right).$$

Then, in the case of straight edges, (1.12) leads to

$$(1.14) \quad u(x, y) = \sum_{j=1}^n \int_{-1}^1 \left[ G \frac{\partial u}{\partial \mathcal{N}} |h_j| + iu \left( \frac{\partial G}{\partial \zeta(t)} h_j - \frac{\partial G}{\partial \bar{\zeta}(t)} \bar{h}_j \right) \right] dt.$$

Given the approximations (1.7), we demonstrate a fast method for computing the right-hand side of (1.14) accurately, given the approximation (1.7), even for large  $N$ , with rapid convergence to the true solution (see Theorem 2.7 and the pseudocode in the appendix). We use a Chebyshev interpolation and convert to Legendre expansions to compute the relevant integrals. In the particular case of Laplace’s equation, the approximate representation can be given *explicitly* in terms of hypergeometric functions.

- We use these ideas to extend these results theoretically and numerically to domains with *curved edges*.
- We provide several numerical examples showing that the unified transform coupled with the evaluation of (1.14) yields a high order method which is very easy to implement and fast. We also include comparisons with spectral methods.

- Finally we show that the method can deal with corner singularities through the addition of global singular functions to the basis.

An alternative approach for computing the solution inside a convex polygon, where instead of using the integral representation (1.12), the integral representations of [28, 58] were used, was presented in [21] (see Appendix C). The approach presented here appears to be more accurate and efficient; comparisons are made in section 3.1.

The method proposed in this paper has the following attractive features:

- *Very easy to program.* The code required to run the method is very simple, and all our examples were run in MATLAB. (Code will be made available on the first author's website).
- *Speed.* The method is fast. Our numerical experiments were performed on a slow four-year-old laptop with 1.80 GHz processor. For our simple code, the time taken to approximately invert the Dirichlet-to-Neumann map is of the order of a few tens of milliseconds and evaluation at several hundred points in the interior of the order of at most a second. The method is also entirely local and trivially parallelizable.
- *Accurate.* The method converges spectrally for analytic solutions and converges with high algebraic rates for nonsmooth solutions (in the sense that we found faster rates of convergence in the domain interior than along the boundary when corner singularities are present). In fact, we prove that it is only the convergence of the first few coefficients of the Legendre expansion that really matter (Theorem 2.7). As a consequence, we found that the method converges at a much faster rate than spectral methods using polynomials of the same degree.
- *Boundary discretization.* The only approximation occurs at the expansion of the boundary values in terms of Legendre polynomials (or the additional global basis functions capturing corner singularities). A key advantage of the unified transform over boundary element methods is that it is a boundary-based method that avoids entirely the computation of singular integrals [50].

We should remark that one of the reasons for the popularity of boundary integral/element methods is that they typically yield well-conditioned linear systems. A good choice of collocation points is crucial in order for the unified transform to be well-conditioned as further discussed in [35]; the choice (1.11) leads to a diagonally dominant linear system. It is also crucial to overdetermine the system ( $M > N$ ) (also explored in [63] in the context of the water wave problem).

Of course, in the presence of corner singularities the choice of Legendre functions as a basis can only achieve algebraic rates of convergence along the boundary. However, the evaluation of (1.14) in the interior of the domain is found to converge more rapidly than the evaluation of the missing boundary values via the global relation. We also found that weak singularities are not a serious problem for the computation of the solution in the domain interior, despite degrading the accuracy of the approximation of the Dirichlet-to-Neumann map. In particular, we refer the reader to Theorem 2.7 and the error plots in Figure 6 and Figure 7.

Additionally, a procedure for adapting the basis to cope with corner singularities for evaluating the Dirichlet-to-Neumann along  $\partial\Omega$  was discussed in [33, 16]. Adding global basis functions consisting of singular functions to our original local basis improves the method, and one can still benefit from applying the numerical method for computation of the relevant integrals in this paper to the local basis approximating the smooth part of the solution in the domain interior (see the example in section 3.4).

While we adopt a global basis approach to singularities, further methods designed to cope with corner singularities are extensively reviewed in [40, 47].

**Organization of the paper.** In section 2 we give expressions for approximations of the solution in the interior using the unified transform and expansions (1.7). We also present our numerical method of computing the relevant integrals quickly and accurately. The ideas presented in this section are also shown to allow the numerical implementation of the unified transform in domains with curved boundaries in section 3.3. Numerical examples of each equation are shown in section 3 where we also compare against spectral methods. Finally, conclusions as well as remaining challenges of the method and future work are discussed in section 4. An appendix proving the results of section 2 is also given, as well as pseudocode for our numerical method.

**2. Approximations in the interior.** In this section we shall show how the expansions of the boundary data and computed boundary values give rise to approximations of the solution in the interior. This can be achieved by inserting the computed approximations into (1.14). For the sake of simplicity, we shall stick to convex domains with straight edges and discuss extensions in section 3. We begin with deriving integral expressions for the solutions, which in the particular case of Laplace’s equation can be written explicitly in terms of hypergeometric functions. We then discuss a fast and accurate numerical method for the evaluation of the relevant integrals.

**2.1. Integral expressions.** The following propositions give the relevant integral expressions for the solution in terms of the approximated boundary values.

PROPOSITION 2.1 (Laplace). *Let  $u$  satisfy the Laplace equation in the interior of a convex polygon specified by the corners  $\{z_j\}_1^n$ . Let  $u_j$  and  $\frac{\partial u_j}{\partial N}$  be approximated by (1.7). For a well-posed problem the algorithm presented in section 1 determines the constants  $\{a_l^j, b_l^j\}$ . Substituting these expansions into (1.14) gives the approximation*

$$(2.1) \quad u(x, y) \approx \sum_{j=1}^n |h_j| \sum_{l=0}^{N-1} b_l^j J_l^j + \sum_{j=1}^n h_j \sum_{l=0}^{N-1} a_l^j I_l^j + \sum_{j=1}^n \bar{h}_j \sum_{l=0}^{N-1} a_l^j \bar{I}_l^j,$$

where the following representations are valid for  $J_l^j$  and  $I_l^j$ .

$$(2.2) \quad J_l^j = -\frac{1}{2\pi} \int_{-1}^1 \ln(|z - m_j - h_j t|) P_l(t) dt, \quad l = 0, 1,$$

which simplifies to

$$(2.3) \quad J_0^j = -\frac{1}{2\pi} \left( \ln |(z - m_j)^2 - h_j^2| + \operatorname{Re} \left\{ -2 + \frac{z - m_j}{h_j} \ln \frac{z - m_j + h_j}{z - m_j - h_j} \right\} \right),$$

$$(2.4) \quad J_l^j = \frac{\Gamma(l+1)^2}{\pi l} \operatorname{Re} \{ \eta_j^l {}_2\tilde{F}_1(l, l+1; 2l+2; \eta_j) \}, l > 0,$$

and

$$(2.5) \quad I_l^j = \frac{i}{4\pi} \int_{-1}^1 \frac{P_l(t) dt}{z - m_j - h_j t} = \frac{i}{4\pi h_j} \Gamma(l+1)^2 \eta_j^{l+1} {}_2\tilde{F}_1(l+1, l+1; 2l+2; \eta_j).$$

In the above formulae,  ${}_2\tilde{F}_1(a, b; c; z)$  denotes the regularized hypergeometric function,  $\eta_j = \frac{2h_j}{z - m_j + h_j}$ , and  $h_j, m_j, z, \bar{z}$  are defined by

$$(2.6) \quad h_j = \frac{z_{j+1} - z_j}{2}, \quad m_j = \frac{z_{j+1} + z_j}{2}, \quad z = x + iy, \quad \bar{z} = x - iy.$$

PROPOSITION 2.2 (modified Helmholtz). *Let  $u$  satisfy the modified Helmholtz equation (1.1) in the interior of a convex polygon specified by the corners  $\{z_j\}_1^n$ . Let  $u_j$  and  $\frac{\partial u_j}{\partial N}$  be approximated by (1.7). For a well-posed problem the algorithm presented in section 1 determines the constants  $\{a_l^j, b_l^j\}$ . Using (1.14), this gives the approximation*

$$(2.7) \quad \begin{aligned} u(x, y) \approx & \frac{1}{2\pi} \sum_{j=1}^n |h_j| \sum_{l=0}^{N-1} b_l^j \int_{-1}^1 K_0(\kappa|z - m_j - th_j|) P_l(t) dt \\ & - \frac{\kappa}{2\pi} \sum_{j=1}^n |h_j| \sum_{l=0}^{N-1} a_l^j \int_{-1}^1 \operatorname{Re} \left\{ \left[ -\frac{\bar{h}_j(z - m_j - th_j)}{h_j(\bar{z} - \bar{m}_j - t\bar{h}_j)} \right]^{\frac{1}{2}} \right\} K_1(\kappa|z - m_j - th_j|) P_l(t) dt, \end{aligned}$$

where  $h_j, m_j, z, \bar{z}$  are defined in (2.6) and  $K_n(z)$  denotes the modified Bessel function of the second kind.

Remark 2.3. The representation obtained in Proposition 2.1 for the Laplace equation can be obtained by letting  $\kappa \rightarrow 0$  in Proposition 2.2 assuming the condition

$$(2.8) \quad \sum_{j=1}^n |h_j| b_0^j = 0,$$

which corresponds to the vanishing of the integral of the normal derivative along the boundary. The fact that this condition is indeed valid for a solution of the Laplace equation can be seen by applying the divergence theorem to the integral of  $\nabla^2 u$  over the domain.

PROPOSITION 2.4 (Helmholtz). *Let  $u$  satisfy the Helmholtz equation (1.1) in the interior of a convex polygon specified by the corners  $\{z_j\}_1^n$ . Let  $u_j$  and  $\frac{\partial u_j}{\partial N}$  be approximated by (1.7). For a well-posed problem the algorithm presented in section 1 determines the constants  $\{a_l^j, b_l^j\}$ . Using (1.14), this gives the approximation*

$$(2.9) \quad \begin{aligned} u(x, y) \approx & \frac{i}{4} \sum_{j=1}^n |h_j| \sum_{l=0}^{N-1} b_l^j \int_{-1}^1 H_0^{(1)}(\kappa|z - m_j - th_j|) P_l(t) dt \\ & - \frac{i\kappa}{4} \sum_{j=1}^n |h_j| \sum_{l=0}^{N-1} a_l^j \int_{-1}^1 \operatorname{Re} \left\{ \left[ -\frac{\bar{h}_j(z - m_j - th_j)}{h_j(\bar{z} - \bar{m}_j - t\bar{h}_j)} \right]^{\frac{1}{2}} \right\} H_1^{(1)}(\kappa|z - m_j - th_j|) P_l(t) dt, \end{aligned}$$

where  $h_j, m_j, z, \bar{z}$  are defined in (2.6) and  $H_n^{(1)}(z)$  denotes the Hankel function.

Remark 2.5. Proposition 2.4 also follows from Proposition 2.2 by using the substitution  $\kappa \rightarrow -i\kappa$  and the following identity which is valid for  $-\pi < \arg(x) \leq \pi/2$ :

$$(2.10) \quad K_\alpha(x) = \frac{\pi}{2} i^{\alpha+1} H_\alpha^{(1)}(ix).$$

Remark 2.6. To obtain real solutions of the Helmholtz equation, we can use the real part of the fundamental solution. Thus, for real solutions,  $iH_0^{(1)}$  and  $iH_1^{(1)}$  in (4.6) are replaced by their respective real parts (this corresponds to taking the real part of the approximate form of  $u$ ).

**2.2. Numerical method.** There are two main sources of difficulty in numerically computing the relevant integrals in Propositions 2.1, 2.2, and 2.4. First, the integrals become highly oscillatory if the degree of the Legendre polynomial is large, and, second, they become more difficult to evaluate close to the boundary as the integrand becomes more singular. Here we show that the first of these difficulties can be overcome by the use of Chebyshev interpolation, allowing us to treat large  $N$  rapidly and accurately. We also demonstrate that the second difficulty only occurs very near to corner points, and this is not an issue in practice (see section 3.2). It is important to note that the method described here also allows easy implementation of the unified transform in domains with curved boundaries (see section 3.3), but since the numerical method is essentially the same, we only discuss how to compute the integrals in section 2.1.

First, we have the following simple theorem which suggests that only the approximation of the first few Legendre coefficients really matters (this is important when we discuss an example which includes a corner singularity). It suggests the approximation in the interior converges at least as fast as the global relation along the boundary (we have actually found it to be faster in practice).

**THEOREM 2.7.** *Suppose that we approximately solve (1.1) to obtain (1.7):*

$$(2.11) \quad u_j(t) \approx \sum_{l=0}^{N-1} a_l^j P_l(t), \quad \frac{\partial u_j}{\partial N}(t) \approx \sum_{l=0}^{N-1} b_l^j P_l(t), \quad j = 1, \dots, n, \quad t \in [-1, 1].$$

*Suppose also that along the boundary the true solution  $u$  and its normal derivative lie in  $H^s(\partial\Omega)$  for some  $s \geq 0$  and we approximate the coefficients  $a_l^j, b_l^j$  for  $l \leq N - 1, j = 1, \dots, n$  to an accuracy  $\epsilon$ . Given any compact subset  $K \subset \Omega$  and the approximate solution  $u_{\text{approx}}$  obtained via Propositions 2.1, 2.2, and 2.4, respectively, there exist constants  $C_1, C_2$  dependent only on  $u, \Omega$ , and  $K$  and a constant  $\rho > 0$  dependent only on  $u$  such that*

$$(2.12) \quad \|u - u_{\text{approx}}\|_{\infty, K} \leq C_1 N \epsilon + C_2 N^{-s} e^{-N\rho},$$

where  $\|\cdot\|_{\infty, K}$  denotes the supremum norm over the compact set  $K$ .

**Remark 2.8.** The condition that the Dirichlet and Neumann values lie in  $H^s(\partial\Omega)$  is not restrictive for convex  $\Omega$  for smooth enough boundary data (the corner singularities that could arise have boundary data in some  $H^s(\partial\Omega)$  [39, 17]). For nonconvex domains this is more restrictive, but one can supplement the Legendre basis with singular functions and apply the above theorem to the smoother part.

**2.3. Integrals for the Laplace equation.** For simplicity, consider first the evaluation of the integrals for Laplace’s equation, where after letting  $\alpha + i\beta = (z - m_j)/h_j$  we are led to the evaluation of the following integrals:

$$A_m(\alpha, \beta) = \int_{-1}^1 P_m(t) \ln(\sqrt{(\alpha - t)^2 + \beta^2}) dt, \quad B_m(\alpha, \beta) = \int_{-1}^1 P_m(t) \frac{\beta}{(\alpha - t)^2 + \beta^2} dt.$$

These integrals were considered in [33] for a boundary integral method at points along  $\partial\Omega$  where a recurrence relation was derived based on the recurrence relations of the Legendre polynomials and integration by parts. Unfortunately such recurrence relations cannot be easily obtained for the modified Helmholtz and Helmholtz equations and become unstable for large  $\beta$  (or near the corners  $\alpha = \pm 1, \beta = 0$ ). Hence, the use

of such relations for evaluating the integrals in the interior of the domain is limited. Proposition 2.1 allows us to represent the integrals  $A_m$  and  $B_m$  exactly in terms of hypergeometric functions. In what follows we have computed these hypergeometric functions to machine precision, allowing us to compute errors of the various approximations.

The integrals of interest are simply rescaled Legendre coefficients of certain functions analytic in a neighborhood of the interval  $[-1, 1]$ . Hence we compute the Legendre coefficients of  $\ln(\sqrt{(\alpha - t)^2 + \beta^2})$  and  $\frac{\beta}{(\alpha - t)^2 + \beta^2}$  through first computing a high order Chebyshev interpolation and then converting the approximated Chebyshev coefficients to Legendre coefficients. An  $M$ -point Chebyshev interpolation can be formed by evaluating at the zeros (or extrema) of the  $(M + 1)$ th Chebyshev polynomial. The interpolation is also numerically stable [36, 26] and can be done extremely efficiently using the FFT (even to millions of interpolation points [59]). Computing Legendre coefficients this way has been used in [2, 49] leading to an  $\mathcal{O}(M \log(M)^2)$  algorithm. This is not quite optimal; specifically, in [37] the existence of a  $\mathcal{O}(M \log(M))$  algorithm was established. The functions we deal with are analytic in a neighborhood of  $[-1, 1]$  and hence the Chebyshev interpolation converges exponentially in the supremum norm over  $[-1, 1]$  [59, 22]. Assuming the error in the conversion from Chebyshev to Legendre coefficients to be negligible, it follows that the error in approximating the sought integrals  $A_m, B_m$  is bounded by  $2/(2m - 1)$  times the error of the Chebyshev interpolate and hence should rapidly decrease as we increase the degree of interpolation. In all the numerical experiments in this paper, we took the number of interpolation points large so that the error of interpolation was of the order of machine precision. For the convenience of the reader, and to demonstrate the simplicity of the method, we have shown a pseudocode for the proposed method in an appendix.

Figure 1 shows the absolute error in computing a range of  $A_m(\alpha, \beta)$  and  $B_m(\alpha, \beta)$  using three different methods: the proposed Chebyshev coefficient method, quadrature using the `quadgk` command in MATLAB, and the recurrence relations in [33]. The recurrence relation becomes unstable away from the boundary (i.e., larger  $\beta$ ), whereas

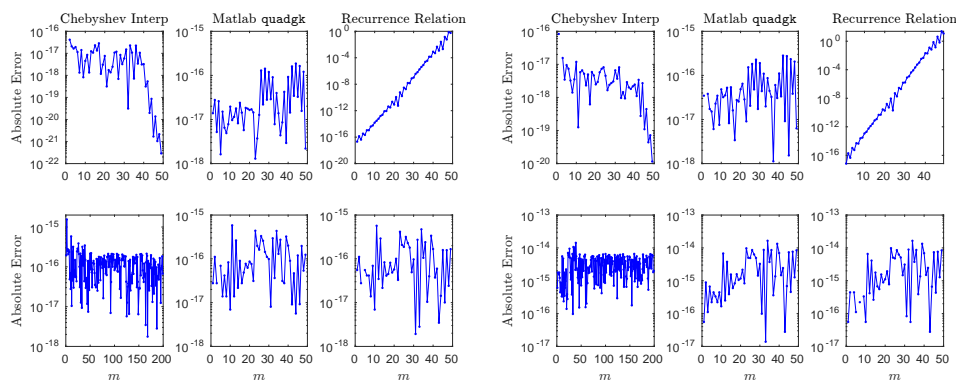


FIG. 1. Absolute errors in approximating the integrals  $A_m$  (left) and  $B_m$  (right) via three methods. The top row is for  $\alpha = 0.1, \beta = 1$  and the bottom row for  $\alpha = 0.1, \beta = 0.01$ . The Chebyshev coefficient method is chosen for its numerical stability and speed. When approximating for  $\alpha = 0.1, \beta = 1$  via the Chebyshev coefficient method, we have not shown larger  $m$  since the values of the integrals are 0 to machine precision. Comparable errors were found when using the Chebyshev coefficient method for larger  $m \sim 1000$ .

quadrature or the Chebyshev coefficient method yields near machine precision. For the evaluation of 50 coefficients and a given  $\alpha, \beta$ , the times taken on laptop with a 1.80 GHz processor for each method were of order 0.01s, 10s, and 0.001s respectively. This change in time becomes more drastic for larger  $m$  (making quadrature evaluation at a large number of points impractical for  $m > 100$ ), whereas there is negligible change in the time taken for the Chebyshev coefficient method. In particular, for a given  $z$  we obtain all the integrals for  $m = 0, \dots, N - 1$  *simultaneously*. Away from the boundary we were able to obtain machine precision using the Chebyshev coefficient method even for  $m \sim 1000$  for a range of  $\alpha$  and  $\beta > 0.001$  (of course for fixed  $\alpha$  and  $\beta$ , the integrals decay exponentially with  $m$ ). For points very close to the boundary the number of Chebyshev coefficients needed is very large (we only found this to be a problem for  $\beta < 0.001$ ), and we must resort to quadrature due to the lack of recurrence relations for the modified Helmholtz and Helmholtz integrals. This is discussed further in section 3.2.

**2.4. Integrals for the modified Helmholtz and Helmholtz equations.**

For the modified Helmholtz and Helmholtz equations, we are led to the evaluation of the following integrals:

(2.13)

$$C_m(\kappa; z - m_j, h_j) := \int_{-1}^1 K_0(\kappa|z - m_j - th_j|) P_m(t) dt,$$

(2.14)

$$D_m(\kappa; z - m_j, h_j) := \int_{-1}^1 \operatorname{Re} \left\{ \left[ -\frac{\bar{h}_j(z - m_j - th_j)}{h_j(\bar{z} - \bar{m}_j - t\bar{h}_j)} \right]^{\frac{1}{2}} \right\} K_1(\kappa|z - m_j - th_j|) P_m(t) dt,$$

(2.15)

$$E_m(\kappa; z - m_j, h_j) := \int_{-1}^1 H_0^{(1)}(\kappa|z - m_j - th_j|) P_m(t) dt,$$

(2.16)

$$F_m(\kappa; z - m_j, h_j) := \int_{-1}^1 \operatorname{Re} \left\{ \left[ -\frac{\bar{h}_j(z - m_j - th_j)}{h_j(\bar{z} - \bar{m}_j - t\bar{h}_j)} \right]^{\frac{1}{2}} \right\} H_1^{(1)}(\kappa|z - m_j - th_j|) P_m(t) dt.$$

We compared the reconstructed functions using the computed Legendre coefficients to the original function by measuring the relative  $L^\infty$  error over 100 evenly spaced points in the interval  $[-1, 1]$ . (This is obtained by dividing the  $L^\infty$  error by the supremum of the magnitude of function over the interval.) Figure 2 shows the results over a range of  $\kappa$  using the first 401 Legendre coefficients and  $z - m_j = 0.1i$ ,  $h_j = 1$ . This demonstrates that the integrals can be computed accurately and efficiently, even for large  $m$ . We have also shown a plot for the first 1201 coefficients, showing that quite large  $\kappa$  do not cause any problems.

**3. Numerical results.** We now present numerical examples of the method.

The time taken to compute the unknown expansion coefficients in our examples is typically a few tens of milliseconds while the solution in the interior can be computed at several hundred points in the order of a second. As mentioned in section 2, since we interpolate to machine precision and obtain all the relevant integrals at once, the time taken for the evaluation is virtually independent of  $N$ ; hence, we have not plotted time as a function of  $N$ .

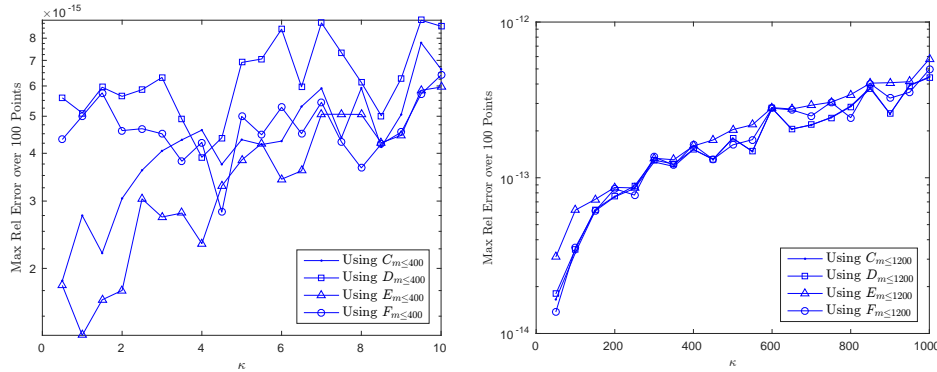


FIG. 2. Left: Discrete relative  $L^\infty$  error for the reconstructed functions using  $C_m$ ,  $D_m$ ,  $E_m$ , and  $F_m$  for a range of  $\kappa$ . The small errors indicate that the integrals can be computed accurately for large  $m$ . Right: Similar plots but now for larger  $\kappa$  using the first 1201 coefficients.

We begin with examples of the Helmholtz and modified Helmholtz equations, comparing the proposed method to evaluations using the integral representations of the unified transform that have appeared in [56, 58] and numerically implemented in [21]. We then conclude the discussion of section 2 by considering points close to the boundary. Our final examples consider Laplace’s equation. We begin with an example containing a weak corner singularity demonstrating Theorem 2.7 and also that the ideas of this paper can be adapted to treat domains with *curved* edges. We then conclude this section with a more singular problem, demonstrating how global singular functions can be added to the basis to improve the method.

**3.1. Helmholtz and modified Helmholtz.** We first consider smooth solutions to the Helmholtz and modified Helmholtz equations in order to compare our method to that of [56, 58] which gave rise to a novel integral representation of the solution. The method of [56, 58] computes the solution  $u$  via integrating the spectral data  $\hat{u}_j$  (computed via the same collocation method as outlined in the introduction) on rays in the complex plane extending to infinity, and, for completeness, details can be found in Appendix C.

The domain considered is shown in the left of Figure 3 with corners  $(z_1, z_2, z_3, z_4) = (0, 1, 1 + 2i, i)$ . For the modified Helmholtz equation, the relevant solution is

$$(3.1) \quad u(x, y) = \text{Im} \left( \exp \left( z + \frac{\kappa^2}{4} \bar{z} \right) \right).$$

We choose  $\kappa = 1$  consistent with [21], and for given Dirichlet boundary data we compute the solution for parameter choices  $R = 10N$  and  $M = 5N$  in (1.11). For the Helmholtz equation, we take

$$(3.2) \quad u(x, y) = \text{Re} \left( \sum_{m=0}^{\infty} (-2)^{-m} \exp[i\kappa(\cos(m)x + \sin(m)y)] \right)$$

with  $\kappa = 5$  and consider given Neumann boundary data along side  $\Gamma_1$  and Dirichlet data along the other sides.

The approximate spectral data  $\hat{u}_j$  computed numerically via the inversion of the Dirichlet-to-Neumann map are given in terms of modified Bessel functions by (1.10). This makes numerically integrating the spectral data along the relevant rays

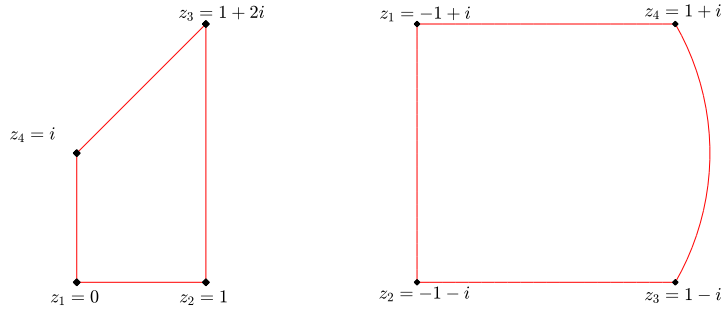


FIG. 3. Left: Trapezoidal domain. Right: Domain with curved boundary  $\Gamma_3$ . We use the parameter  $\mathcal{R}$  for the radius of curvature, with  $\mathcal{R} = \infty$  a square.

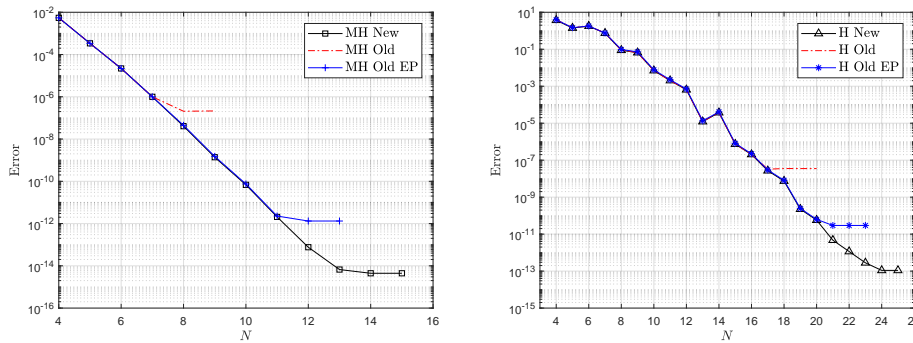


FIG. 4. Left: Errors of new method compared to old method in [56, 58, 21] for the modified Helmholtz equation. EP stands for extended precision. The condition number of the linear system, used to compute unknown boundary coefficients, was bounded by 100 for all  $N$  considered. Right: Same but for the Helmholtz equation.

difficult for large and small spectral arguments. Hence we have also compared with the numerical evaluation of these Bessel functions in extended precision for the relevant quadrature. The absolute errors are shown in Figure 4 over a Cartesian grid (with respect to the  $(x, y)$  variables) of side length 0.01 covering the domain.<sup>2</sup> Note that the proposed method achieves errors several orders of magnitude smaller than that of the method in [56, 58], even when using extended precision for the spectral data. This agrees with the errors of the  $10^{-11}$  reported in [21] for the above modified Helmholtz example when using the *exact* spectral data (which for this example have a simple form). Our proposed method is not only numerically more accurate but is also much simpler/faster to implement.

**3.2. Points near  $\partial\Omega$ .** Here we supplement the discussion of section 2 by considering points close to the boundary. It is well known that solutions expressed as layer potentials become numerically inaccurate close to the boundary. A possible way around this via local Taylor expansions is discussed in [12]. However, we demonstrate that this is not needed for our proposed method—the errors only become an issue very close to the corners, to the extent that one can use the first order approximation in this regime (together with the computed Dirichlet/Neumann boundary values), and

<sup>2</sup>From now on we will refer to such a collection simply as a grid.

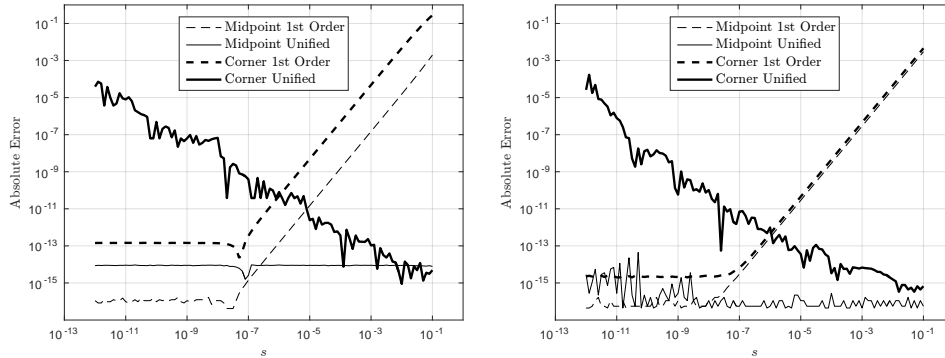


FIG. 5. *Left: Comparison of using first order approximation and hypergeometric functions with the unified transform for points close to  $z_1$  and at the midpoint of  $\Gamma_1$  for Laplace with  $N = 40$ . Right: Similar plots but for modified Helmholtz using quadrature and for points close to  $z_4$  and at the midpoint of  $\Gamma_4$  with  $N = 20$ .*

are not an issue for the case of approximating near the midpoints of the sides of the polygon.

Using quadrature (or the hypergeometric functions in the case of Laplace) to evaluate the relevant integrals, we compute the errors of approximating  $u = \text{Re}\left(\frac{ze^{z^3}}{z-(2i+1)}\right)$  (Laplace). The domain considered, also used in section 3.3, is shown in the right of Figure 3 and has a curved boundary  $\Gamma_3$  of constant radius of curvature  $\mathcal{R}$ . For now, we take  $\mathcal{R} = \infty$ , corresponding to a square domain with straight edges, with mixed boundary data  $u_1, \partial u_2/\partial \mathcal{N}, u_3,$  and  $\partial u_4/\partial \mathcal{N}$ . We also consider the example given above for the modified Helmholtz. We consider the errors of the computed solution approaching a corner  $z_j$  diagonally (bisecting its internal angle denoted  $\alpha_j$ ) and approaching the midpoint of side  $\Gamma_j$  perpendicularly. Denoting the distance to the boundary along such a path by  $s$ , we compare with the error obtained via the simple first order approximations,

$$u_j(-1 + s \cos(\alpha_j/2)/|h_j|) - s \sin(\alpha_j/2) \frac{\partial u_j}{\partial \mathcal{N}}(-1 + s \cos(\alpha_j/2)/|h_j|) \quad (\text{corners})$$

$$u_j(0) - s \frac{\partial u_j}{\partial \mathcal{N}}(0) \quad (\text{midpoints}).$$

These expressions are computed using the boundary data (half given and half obtained via the unified transform). Figure 5 shows the results for  $N = 40$  (Laplace) and  $N = 20$  (modified Helmholtz). As expected, the first order approximations break down when  $s^2$  is approximately the error in the computation at interior points. Similar results were found for other boundary points and larger  $N$ .

**3.3. Laplace: Weak singularities and curved domains.** We will consider a solution with a corner singularity (so the Legendre basis will only give algebraic convergence) to demonstrate Theorem 2.7 and also how the algorithm in section 2 can be used to treat curved boundaries. Suppose the side  $\Gamma_j$  is parametrized as

$$[-1, 1] \ni t \rightarrow x_j(t) + iy_j(t), \quad x_j(t), y_j(t) \in \mathbb{R}.$$

Introduce the quantity  $l_j(t) = \sqrt{\dot{x}_j(t)^2 + \dot{y}_j(t)^2}$  along the curve (where the dot denotes differentiation with respect to  $t$ ), and let  $(n_1(t), n_2(t))^T$  be the outward normal. Then, the integral transform in (1.3) becomes

$$(3.3) \quad \hat{u}_j(\lambda) = \int_{-1}^1 e^{-i\lambda z(t)} \left[ \frac{\partial u_j}{\partial \mathcal{N}} + \lambda u_j(n_1(t)i - n_2(t)) \right] l_j(t) dt$$

$$(3.4) \quad \approx \sum_{l=0}^{N-1} \int_{-1}^1 e^{-i\lambda z(t)} \left[ b_l^j P_l(t) + \lambda(n_1(t)i - n_2(t)) a_l^j P_l(t) \right] l_j(t) dt.$$

We can then use the algorithm of section 2 to accurately compute numerically these integrals and set up the approximate global relation. The relation (1.12) then becomes

$$(3.5) \quad u(x, y) = \sum_{j=1}^n \int_{-1}^1 \left[ G \frac{\partial u_j}{\partial \mathcal{N}} + i u_j \left( \frac{\partial G}{\partial \zeta(t)} (n_1(t)i - n_2(t)) + \frac{\partial G}{\partial \bar{\zeta}(t)} (n_1(t)i + n_2(t)) \right) \right] l_j(t) dt,$$

which again can be approximated using the expansions (1.7) and the methods of section 2 (see also the appendix). The numerical method we present can be adapted to *general* curved boundaries, but it is worth remarking that an extension of the Fourier transform pair for circular-arc polygons was presented in [18, 19, 41] which extends the unified transform representations in Appendix C.

The domain we consider is shown in the right of Figure 3, where, for simplicity,  $\Gamma_3$  has constant radius of curvature  $\mathcal{R}$ . When the curvature  $\mathcal{R} = \infty$  (i.e., a square), the strongest corner singularity (for  $H^1(\Omega)$  solutions) with smooth Dirichlet data is of the form

$$(3.6) \quad u(x, y) = r^2 (\log(r) \sin(2\theta) + \theta \cos(2\theta)),$$

where  $(r, \theta) = (\sqrt{(x+1)^2 + (y+1)^2}, \tan^{-1}[(y+1)/(x+1)])$  denotes polar coordinates centred at  $z_2$ . We take this as our reference solution and illustrate the method with Dirichlet data. For collocation points we took  $20N$  Halton nodes<sup>3</sup> (unless stated, all experiments used collocation points described in step (iv) in the introduction) within a (complex) disk of radius 40. This ensures that the collocation points  $\lambda$  do not produce test functions which oscillate too wildly (these would require a very large number of Chebyshev coefficients to compute the integrals in the global relation via the above method).

Figure 6 shows the convergence of the unified transform, both in the interior (where we measure the absolute error on a uniform grid of side length 0.05) and along the boundary (the  $l^2$  error of computed coefficients). As expected, we only see algebraic convergence. We have also included a reference line of slope  $-12$ ; this was approximately the convergence rate of the first few Legendre coefficients, and we expect this to dominate the error in this approximation (see Theorem 2.7). This is also captured by the agreement for small  $N$  between internal and boundary errors. In general, we have found this to be the case for a range of examples with different types of singularities and given boundary data. Note that the rate of convergence for this example is faster than the optimal rate of convergence along the boundary for the boundary values. It can be shown [10] that up to logarithmic factors, the rate of convergence of the Legendre expansion of the Neumann boundary values in

---

<sup>3</sup>These create scattered points with a lack of regularity and can be easily generated in MATLAB. They provide an example of a quasi-random number sequence and are used in the theory of numerical integration [45].

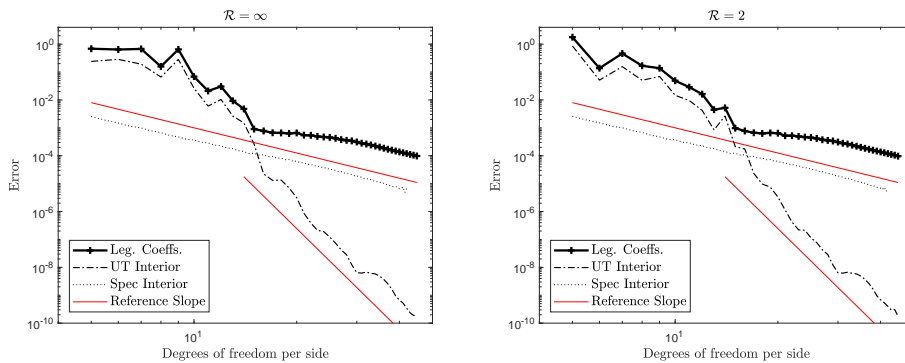


FIG. 6. *Left: Errors for unified transform and spectral method for the square. Right: Same but for  $\mathcal{R} = 2$ .*

$L^2(\partial\Omega)$  is  $N^{-3}$  (also shown as reference). Integrating against an analytic function in the representation (2.1) causes the method to converge faster in the interior than on the boundary itself. Note also that the presence of the curved boundary makes negligible difference to the accuracy of the method. The choice of Halton nodes as collocation points, as opposed to the rays in (1.11), led to a larger condition number of about  $10^4$  for  $N = 40$ , with very little difference between the case of straight and curved boundaries.

Finally, we have also compared the unified transform to a very simple spectral collocation method in Figure 6. This spectral method simply expands the solution in the harmonic functions  $\{1, \operatorname{Re}(z^k), \operatorname{Im}(z^k)\}$  and collocates along the boundaries. For collocation points we took Chebyshev nodes along each side  $\Gamma_i$  to determine the unknown coefficients. Of course a better choice of basis can be chosen with knowledge of the particular type of corner singularities expected (as we demonstrate below), but Figure 6 demonstrates some interesting points. It appears that the use of the harmonic polynomial basis causes the spectral method to converge at the same rate as the Legendre expansion of the unknown Neumann boundary values. It is also apparent that there is a significant advantage of approximating just the boundary values, using Green's representation formula and Theorem 2.7. Both the unified transform and the spectral method use a polynomial basis, yet the locality of the unified transform leads to a much more accurate method (and faster rates of convergence) in the domain's interior.

**3.4. Laplace: Strong singularities and singular functions.** Our final example considers Laplace's equation for the mixed BVP shown in Figure 7. Let the angle between  $\Gamma_{j-1}$  and  $\Gamma_j$  be  $\alpha_j\pi$ , and consider local polar coordinates  $(r_j(x, y), \theta_j(x, y))$  centered at  $z_j$  such that  $\Gamma_j$  lies along  $\theta_j = 0$ . We chose  $\alpha_2 \approx 0.7971$ ,  $\alpha_1 = \alpha_3$  and  $|\Gamma_1| = 1$ . In general, the large angle  $\alpha_2\pi$  and mixed boundary conditions induce strong corner singularities. In order to assess our method we chose the test solution

$$(3.7) \quad u(x, y) = \cos(x) \sinh(y) + \sum_{m=1}^{\infty} \left\{ \left( \frac{r_1(x, y)}{3} \right)^{\frac{m}{\alpha_1}} \sin \left( \frac{m}{\alpha_1} \theta_1 \right) + \left( \frac{r_2(x, y)}{4} \right)^{\frac{m-1/2}{\alpha_2}} \cos \left( \frac{m-1/2}{\alpha_2} \theta_2 \right) + \left( \frac{r_3(x, y)}{5} \right)^{\frac{m-1/2}{\alpha_3}} \sin \left( \frac{m-1/2}{\alpha_3} \theta_3 \right) \right\},$$

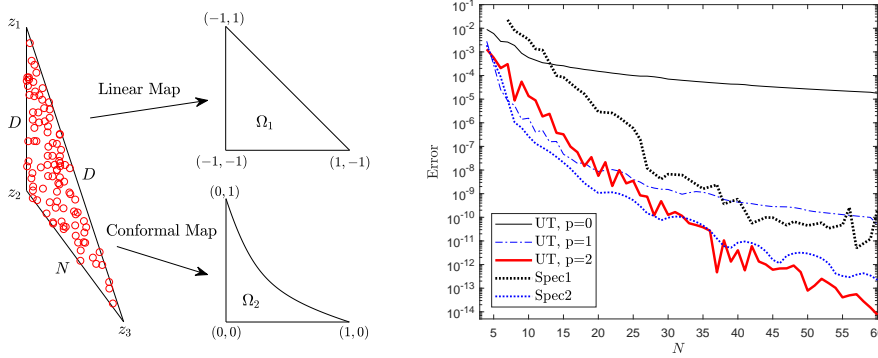


FIG. 7. Left: Triangular domain and random test points.  $D$  and  $N$  stand for given Dirichlet and Neumann boundary data respectively. We have also shown the transformed domain for the spectral method and unified transform combined with a conformal map. Right: Errors for unified transform and spectral methods.

which includes the general form of corner singularities given smooth boundary data (again we assume the solution lies in  $H^1(\Omega)$ ).

To improve the rate of convergence, we have added *global* basis functions of the form  $r_i^\alpha \phi(b\theta_i)$  (where  $\phi$  is the appropriate trigonometric function) to our *local* basis of Legendre polynomials along each side. To implement this we used the formula

$$(3.8) \quad \int_{-1}^1 e^{i\lambda t} (1+t)^\alpha dt = \frac{e^{-i\lambda} \gamma(\alpha+1, -2i\lambda)}{(-i\lambda)^{\alpha+1}},$$

where  $\gamma$  denotes the (lower) incomplete gamma function. Given a global basis function, the relation (3.8) allows us to compute the contribution to the global relations along sides adjacent to the corner where the singularity is centred. Along the other sides, the new basis function and its derivatives are smooth, and hence the contribution to the global relation can be computed using standard Legendre interpolation and (1.10).

Figure 7 shows the maximum error over 100 points in the interior of the domain (chosen uniformly at random and also shown in Figure 7) as a function of  $N$  when we add the  $p$  most singular global functions to our basis. The parameters chosen were  $R = 10N$  and  $M = 5N$ . Including just two singular functions leads to a dramatic increase in the accuracy of the method. We have also compared the unified transform to the simple spectral collocation in section 3.3 (Spec1). However, now we choose the functions  $r_i^\alpha \phi(b\theta_i)$  as well as  $\{1, \text{Re}(z^k), \text{Im}(z^k)\}$  and select the first  $N$  of these with smallest power scale. The spectral method initial converges exponentially for small  $N$ ; however, for large  $N$  it becomes numerically unstable. This is a well-known problem for such methods; see, e.g., [13]. The unified transform is more stable for large  $N$  and is able to obtain more accurate results. However, the condition number of the linear system grows with the addition of singular functions. For  $N = 60$ , the condition numbers were approximately  $5 \times 10^3$ ,  $6 \times 10^4$ , and  $3 \times 10^9$  for  $p = 0, 1$ , and  $2$ , respectively. Though the method appears to be stable from the results of Figure 7, we found that using additional singular functions led to very little improvement of the accuracy of the method. We have also shown the results of a spectral method taken from [38] (Spec2). This considers orthogonal polynomials in the right-angled triangle  $\Omega_1$  in Figure 7 given by

$$(3.9) \quad \phi_{p,q} = P_p^{(0,0)}(\eta_1) \left( \frac{1-\eta_2}{2} \right)^p P_q^{(2p+1,0)}(\eta_2), \quad (\eta_1, \eta_2) = \left( \frac{2(x+1)}{1-y} - 1, y \right),$$

where  $P_n^{(a,b)}$  denote the standard Jacobi polynomials. As well as these polynomials, we added the first two singular functions  $r_i^\alpha \phi(b\theta_i)$  to the basis.<sup>4</sup> For this method the parameter  $N$  corresponds to the maximum degree of the included polynomials. This method is much more stable and well-conditioned compared to the other spectral method at large  $N$ . It is also clear that the unified transform is competitive particularly for large  $N$  and appears to converge at a faster rate, again due to Theorem 2.7. It should also be mentioned that the number of basis functions used in Spec2 is  $N(N+1)/2 + 2$ . Despite the polynomials not being separable, one can still take advantage of the structure to set up the linear system efficiently (see section 4.1.6 of [38]). However, the linear system size grows quadratically in each dimension whereas it only grows linearly for the unified transform. We found that solving the linear system was considerably slower for Spec2 for large  $N$ .

*Remark 3.1.* For this particular problem, another approach is to (approximately) homogenize the boundary conditions locally near  $z_2$  and then remove the dominant corner singularities around  $z_2$  by a conformal mapping of the domain [11, 47], expressed in this case via polar coordinates around  $z_2$  as

$$(r_2, \theta_2) \rightarrow \left( r_2^{\frac{1}{2\alpha_2}}, \frac{\theta_2}{2\alpha_2} \right).$$

This transforms the domain to  $\Omega_2$  in Figure 7 with a curved edge  $\Gamma_3$ , for which the methods of section 3.3 can be applied. We found this to be competitive with the unified transform with  $p = 2$ , though we were only able to obtain errors of around  $10^{-13}$  due to the larger condition number for curved boundaries and the numerical errors in computing the spectral functions.

**4. Conclusion.** It has been established in several publications that the *unified transform* provides an efficient algorithm for computing the so-called generalized Dirichlet-to-Neumann map for linear elliptic PDEs formulated in the interior of a convex bounded polygon. In particular, given Dirichlet or Neumann or Robin data on each of the sides of a polygon, using this algorithm it is possible to find the constant coefficients in the series expansion of Legendre polynomials approximating the associated unknown boundary values on each side. The relevant linear system characterizing these constants has very low condition number [35].

We have shown that the use of a Legendre basis lends itself to efficient computation of the solution in the domain interior. In the case of Laplace's equation, the relevant integrals are given explicitly in terms of regularized hypergeometric functions. For the modified Helmholtz and Helmholtz equations, they can be computed remarkably *fast* and in a *stable* manner even for  $N$  large, using a Chebyshev interpolation scheme. It is interesting to note that once the coefficients have been computed, it is easier and more accurate to compute the integral representation in the interior of the domain in physical space as opposed to Fourier space (see section 3.1). The method also converges more quickly in the interior of the domain than on the boundary and is very easy to implement. The method compares well to a standard spectral method and global singular functions can easily be added to the basis to capture

<sup>4</sup>This only changes the method on the boundary, so it is very easy to incorporate—see [38] for extensive comments on implementation.

corner singularities. In addition, we have demonstrated that our analysis allows the treatment of curved domains and future work will seek to extend this.

The results presented here, may also be significant for the solution of *scattering* problems [15] or the *exterior* problem [4, 57]. It can be shown [32] that in this case the Dirichlet-to-Neumann map for the Laplace, modified Helmholtz, and Helmholtz equations formulated in the exterior of a convex polygon is characterized by letting  $u = 0$  in the left-hand side of (2.1), (2.7), and (2.9), respectively. By choosing appropriate values of  $z$  in the interior of the polygon, it should be possible to determine the expansion coefficients of the unknown boundary values. Then, the appropriately modified global relations [32] yield the scattering amplitudes (this is work in progress). Our approach is also applicable to nonhomogeneous PDEs, as well as to oblique derivative (Poincaré) boundary conditions. Future work will aim at extending the method to three dimensions and higher. Some initial progress in this direction can be found in [3, 1].

**Appendix A. Proofs of results.**

*Proof of Proposition 2.1.* Using the fundamental solution of the Laplace equation,

$$(A.1) \quad G(\xi, \eta; x, y) = -\frac{1}{2\pi} \ln |z - \zeta|, \quad \frac{\partial G}{\partial \zeta} = -\frac{1}{4\pi} \frac{1}{\zeta - z},$$

and letting  $\zeta = m_j + th_j$ , (1.14) becomes

$$u(x, y) \approx -\frac{1}{2\pi} \sum_{j=1}^n |h_j| \sum_{l=0}^{N-1} b_l^j \int_{-1}^1 \ln |z - m_j - th_j| P_l(t) dt + \frac{i}{4\pi} \sum_{j=1}^n h_j \sum_{l=0}^{N-1} a_l^j \int_{-1}^1 \frac{P_l(t) dt}{z - m_j - th_j} - \frac{i}{4\pi} \sum_{j=1}^n \bar{h}_j \sum_{l=0}^{N-1} \bar{a}_l^j \int_{-1}^1 \frac{P_l(t) dt}{\bar{z} - \bar{m}_j - t\bar{h}_j},$$

which is (2.1), with  $J_l^j$  and  $I_l^j$  defined by (2.2) and (2.5), respectively.

In order to derive the alternative formulae for  $I_l^j$ , we first employ Rodrigues' formula, namely,

$$(A.2) \quad P_l(t) = \frac{1}{2^l l!} \left( \frac{d}{dt} \right)^l (t^2 - 1)^l.$$

Substituting this formula into the definition of  $I_l^j$ , we find

$$I_l^j = \frac{i}{2^l l! 4\pi} \int_{-1}^1 \frac{\left( \frac{d}{dt} \right)^l (t^2 - 1)^l}{z - m_j - th_j} dt.$$

Using repeated integration by parts and noting that all boundary terms vanish due to the term  $(t^2 - 1)^l$ , it follows that the operator  $\left( \frac{d}{dt} \right)^l$  finally acts on  $(z - m_j - th_j)^{-1}$ , where it yields the term

$$(-1)^l l! (-h_j)^l (z - m_j - h_j t)^{-(1+l)}.$$

The factor  $(-1)^l$  cancels with the factor  $(-1)^l$  generated by the repeated integration by parts; thus cancelling factorials we obtain

$$I_l^j = \frac{i(-1)^l h_j^l}{2^l 4\pi} \int_{-1}^1 \frac{(t^2 - 1)^l}{(z - m_j - h_j t)^{l+1}} dt.$$

Letting  $t = -1 + 2y$ , we find

$$(A.3) \quad I_l^j = \frac{i2^l h_j^l}{2\pi(z - m_j + h_j)^{l+1}} \int_0^1 \frac{y^l(1 - y)^l}{\left(1 - \frac{2h_j y}{z - m_j + h_j}\right)^{l+1}} dy.$$

Recalling the definition of the regularized hypergeometric function, namely,

$${}_2\tilde{F}_1(a, b; c; z) = \frac{1}{\Gamma(b)\Gamma(c - b)} \int_0^1 \frac{y^{b-1}(1 - y)^{-b+c-1}}{(1 - zy)^a} dy,$$

it follows that

$$(A.4) \quad \int_0^1 \frac{y^l(1 - y)^l}{\left(1 - \frac{2h_j y}{z - m_j + h_j}\right)^{l+1}} dy = \Gamma(l + 1)^2 {}_2\tilde{F}_1(l + 1, l + 1; 2l + 2; \eta_j).$$

Furthermore, the definition of  $\eta_j$  implies

$$(A.5) \quad \frac{1}{(z - m_j + h_j)^{l+1}} = \left(\frac{\eta_j}{2h_j}\right)^{l+1}.$$

Using (2.5) and (A.5) in (A.3) we find (2.5).

In order to derive the alternative formula for  $J_l^j$  we replace in the definition of  $J_l^j$  the term  $P_l(t)$  by the right-hand side of (A.2):

$$(A.6) \quad J_l^j = \frac{-1}{2\pi 2^l l!} \int_{-1}^1 \ln|z - m_j - h_j t| \left(\frac{d}{dt}\right)^l (t^2 - 1)^l dt.$$

If  $l = 0$ , we find

$$(A.7) \quad J_0^j = -\frac{1}{2\pi} \int_{-1}^1 \ln|z - \zeta(t)| dt, \quad \zeta(t) = m_j + h_j t.$$

Employing integration by parts we find

$$(A.8) \quad \int_{-1}^1 \ln|z - \zeta(t)| dt = t \ln|z - \zeta(t)|_{-1}^1 - \int_{-1}^1 \left[ \left(\frac{\partial}{\partial \zeta} \ln|z - \zeta(t)|\right) h_j + \left(\frac{\partial}{\partial \bar{\zeta}} \ln|z - \zeta(t)|\right) \bar{h}_j \right] t dt.$$

Using the equation

$$(A.9) \quad \frac{\partial}{\partial \zeta} \ln|z - \zeta(t)| = -\frac{1}{2} \frac{1}{z - \zeta},$$

(A.8) becomes

$$\int_{-1}^1 \ln|z - \zeta(t)| dt = \ln|z - m_j - h_j| + \ln|z - m_j + h_j| + \operatorname{Re} \int_{-1}^1 \frac{(th_j) dt}{z - m_j - th_j}.$$

Using the identity

$$\int_{-1}^1 \frac{-th_j dt}{z - m_j - th_j} = \int_{-1}^1 \left[ 1 - \frac{z - m_j}{z - m_j - th_j} \right] dt = 2 + \frac{z - m_j}{h_j} \ln \left( \frac{z - m_j - h_j}{z - m_j + h_j} \right),$$

we find

$$\int_{-1}^1 \ln |z - \zeta(t)| dt = \ln |(z - m_j)^2 - h_j^2| + \operatorname{Re} \left\{ -2 + \frac{z - m_j}{h_j} \ln \left( \frac{z - m_j + h_j}{z - m_j - h_j} \right) \right\},$$

and then (A.7) becomes (2.3).

Similarly, integrating by parts the expression (A.6) with  $l \neq 0$  gives

$$(A.10) \quad J_l^j = \frac{-1}{2\pi 2^l l!} \operatorname{Re} \{ h_j \hat{J}_l^j \},$$

where  $\hat{J}_l^j$  is defined by

$$\hat{J}_l^j = \int_{-1}^1 \frac{(\frac{d}{dt})^{l-1} (t^2 - 1)^l}{(z - m_j - h_j t)^l} dt.$$

Proceeding as in the calculation of  $I_l^j$  we find

$$\hat{J}_l^j = (l - 1)! (-h_j)^{l-1} \int_{-1}^1 \frac{(t^2 - 1)^l}{(z - m_j - h_j t)^l} dt.$$

Letting  $t = -1 + 2y$  we find

$$\hat{J}_l^j = \frac{(l - 1)! (-1)^{l-1} h_j^{l-1} 2^{2l+1} (-1)^l}{(z - m_j + h_j)^l} \int_0^1 \frac{y^l (1 - y)^l}{(1 - \eta_j y)^l} dy.$$

The definition of  ${}_2\tilde{F}_1$  implies that the  $y$  integral above equals

$$\Gamma(l + 1) {}_2\tilde{F}_1(l, l + 1; 2l + 2; \eta_j).$$

Substituting the above expression into (A.10) we find (2.4). □

*Proof of Proposition 2.2.* The fundamental solution of the modified Helmholtz equation is given by

$$G(\xi, \eta; x, y) = \frac{1}{2\pi} K_0(\kappa |z - \zeta|),$$

where  $z = x + iy$ ,  $\zeta = \xi + i\eta$ . Using  $\zeta = m_j + th_j$ , we find

$$(A.11) \quad G = \frac{1}{2\pi} K_0(\kappa |z - m_j - th_j|).$$

Employing the identities

$$(A.12) \quad \frac{dK_0(\zeta)}{d\zeta} = -K_1(\zeta), \quad \frac{\partial}{\partial \zeta} |\zeta| = \frac{1}{2} \left( \frac{\bar{\zeta}}{\zeta} \right)^{\frac{1}{2}},$$

we find

$$\frac{\partial G}{\partial \zeta} = -\frac{\kappa}{4\pi} \left( \frac{\bar{\zeta} - \bar{z}}{\zeta - z} \right)^{\frac{1}{2}} K_1(\kappa |\zeta - z|).$$

Thus, letting  $\zeta = m_j + th_j$ , we find

$$(A.13) \quad \frac{\partial G}{\partial \zeta(t)} = -\frac{\kappa}{4\pi} \left( \frac{\bar{z} - \bar{m}_j - t\bar{h}_j}{z - m_j - th_j} \right)^{\frac{1}{2}} K_1(\kappa |z - m_j - th_j|).$$

A similar expression holds for the partial derivative with respect to  $\bar{\zeta}$ . Substituting in (1.14) the expressions for  $u$ ,  $\frac{\partial u}{\partial \bar{N}}$ ,  $G$ ,  $\frac{\partial G}{\partial \zeta}$ ,  $\frac{\partial G}{\partial \bar{\zeta}}$  given by (1.7), (A.11), (A.13), we find (2.7). □

*Proof of Proposition 2.4.* The fundamental solution of the Helmholtz equation is given by

$$(A.14) \quad G(\xi, \eta; x, y) = \frac{i}{4} H_0^{(1)}(\kappa|z - \zeta|) = \frac{i}{4} H_0^{(1)}(\kappa|z - m_j - th_j|).$$

Using the identity

$$\frac{dH_0^{(1)}(\zeta)}{d\zeta} = -H_1^{(1)}(\zeta)$$

and proceeding as in the proof of Proposition 2.2 we find

$$(A.15) \quad \frac{\partial G}{\partial \zeta(t)} = -\frac{i\kappa}{8} \left( \frac{\bar{z} - \bar{m}_j - t\bar{h}_j}{z - m_j - th_j} \right)^{\frac{1}{2}} H_1^{(1)}(\kappa|z - m_j - th_j|).$$

Then, (1.14) yields (2.9). □

*Proof of Theorem 2.7.* Consider the approximate solution  $\tilde{u}$  which occurs when we substitute the exact coefficients  $a_l^j, b_l^j$  into Propositions 2.1, 2.2, 2.4, respectively (i.e., we truncate the Legendre expansions to  $N$  terms). The fundamental solution  $G(x, y; \zeta, \eta)$  and its normal derivatives when evaluated for  $(x, y) \in K$  and  $(\zeta, \eta) \in \partial\Omega$  are uniformly bounded. There are  $\mathcal{O}(N)$  summation terms in the approximations  $\tilde{u}, u_{\text{approx}}$ , and hence there exists  $C_1$  such that

$$\|\tilde{u} - u_{\text{approx}}\|_{\infty, K} \leq C_1 N \epsilon.$$

We also have

$$u(x, y) - \tilde{u}(x, y) = \sum_{j=1}^n \sum_{l=N}^{\infty} \int_{-1}^1 \left[ G|h_j|b_l^j + i \left( \frac{\partial G}{\partial \zeta(t)} h_j - \frac{\partial G}{\partial \bar{\zeta}(t)} \bar{h}_j \right) a_l^j \right] P_l(t) dt.$$

It is well known [14] that for any  $s \geq 0$ , if  $F \in H^s((-1, 1))$  and  $P_N$  denotes the orthogonal projection onto the first  $N$  Legendre polynomials that there exists a constant  $C$  with  $\|F - P_N F\|_2 \leq CN^{-s}$ . It follows that there exists some  $C$  such that

$$|a_l^j| \leq Cl^{-s}, |b_l^j| \leq Cl^{-s}, j = 1, \dots, n.$$

Now the integrals

$$(A.16) \quad \int_{-1}^1 GP_l(t) dt \quad \text{and} \quad \int_{-1}^1 \left( \frac{\partial G}{\partial \zeta(t)} h_j - \frac{\partial G}{\partial \bar{\zeta}(t)} \bar{h}_j \right) P_l(t) dt$$

are simply the (unnormalized) Legendre coefficients of the respective functions. Since the polygon is convex, we can define real analytic branches of these functions for  $(x, y) \in U$  and  $t \in [-1, 1]$ , where  $U$  is an open neighborhood of  $K$  whose closure is contained in  $\Omega$ . It follows that the integrals in (A.16) decay exponentially in  $l$  uniformly over the compact set  $K$  [62]. Hence, by making  $C$  large if necessary,

$$\|u(x, y) - \tilde{u}(x, y)\|_{\infty, K} \leq C \sum_{l=N}^{\infty} l^{-s} e^{-\rho l} \leq N^{-s} e^{-\rho N} \frac{C}{1 - e^{-\rho}}$$

for some  $\rho > 0$ . □

**Appendix B. Pseudocode.**

Here we include pseudocode for the method presented in section 2. Since the method can also be used for curved domains (see section 3.3) we shall be quite general and suppose that we wish to compute the integrals

$$I_n(f) := \int_{-1}^1 f(t)P_n(t)dt, \quad n = 0, \dots, N - 1,$$

simultaneously for a given  $N \in \mathbb{N}$  and function  $f$ . This can be done via the following algorithm. There are many numerical packages that can compute the interpolation (step 1) efficiently, e.g., Chebfun which can be found at <http://www.chebfun.org>.

**Input:**  $N \in \mathbb{N}$ , function handle for  $t \mapsto f(t)$   
**Output:** Vector  $b$ , an approximation of  $\{I_n(f)\}_{n=0}^{N-1}$

- 1 Compute  $M$ -point Chebyshev interpolation of  $f$  and store as vector  $a$  ( $M$  sufficiently large)
- 2 Define  $\Lambda(z) = \Gamma(z + 1/2)/\Gamma(z + 1)$ , where  $\Gamma$  denotes usual gamma function
- 3 Define the matrix  $M \times M$

$$L_{i,j}^M = \begin{cases} 1, & \text{if } i = j = 1 \\ \frac{\sqrt{\pi}}{2\Lambda(i+1)}, & \text{if } 1 < i = j \\ \frac{-(j+1)(i+3/2)}{(i+j+3)(j-i)} \Lambda\left(\frac{j-i-2}{2}\right) \Lambda\left(\frac{j+i+1}{2}\right), & \text{if } 1 < i < j \\ 0, & \text{otherwise.} \end{cases}$$

- 4  $c_j = L(j, :) * a, \quad j = 1, \dots, N$
- 5  $b_j = 2c_j/(2j - 1)$

Note that for  $|z|$  large we can use the well-known asymptotics of  $\Lambda$  to obtain an accurate evaluation.

**Appendix C. Integral representations.**

For completeness, we recall here the integral representations in [56, 58, 21] for which we compare our proposed method against in section 3.1. For simplicity, we shall assume that the domain is a convex polygon and that the solution is real-valued. Non-convex polygons and exterior domains are discussed in detail in [56]. Alternatively, one can split up the nonconvex domain as discussed in [16, 42]. Recall the function  $\hat{u}_j(\lambda)$  defined as the following Fourier transform along the side  $(z_j, z_{j+1})$ :

(C.1)

$$\hat{u}_j(\lambda) = \int_{z_j}^{z_{j+1}} e^{-i\lambda z} \left[ \frac{\partial u_j}{\partial \mathcal{N}} \frac{ds}{dz} + \lambda u_j \right] dz \quad \lambda \in \mathbb{C} \quad (\text{Lap.}),$$

(C.2)

$$\hat{u}_j(\lambda) = \int_{z_j}^{z_{j+1}} e^{\frac{i\kappa}{2} \left( \frac{\bar{z}}{\lambda} - \lambda z \right)} \left[ \frac{\partial u_j}{\partial \mathcal{N}} \frac{ds}{dz} + \frac{\kappa u_j}{2} \left( \lambda + \frac{1}{\lambda} \frac{d\bar{z}}{dz} \right) \right] dz \quad \lambda \in \mathbb{C} \setminus \{0\} \quad (\text{mod. Helm.}),$$

(C.3)

$$\hat{u}_j(\lambda) = \int_{z_j}^{z_{j+1}} e^{\frac{-i\kappa}{2} \left( \lambda z + \frac{\bar{z}}{\lambda} \right)} \left[ \frac{\partial u_j}{\partial \mathcal{N}} \frac{ds}{dz} + \frac{\kappa u_j}{2} \left( \lambda - \frac{1}{\lambda} \frac{d\bar{z}}{dz} \right) \right] dz \quad \lambda \in \mathbb{C} \setminus \{0\} \quad (\text{Helm.}).$$

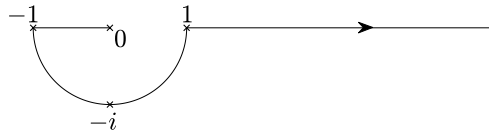


FIG. 8. Contour  $L_{\text{out}}$  used for representation of solution  $u$  of Helmholtz's equation.

For the Laplace and modified Helmholtz equations, let  $l_j$  denote the ray in the complex plane of all points with argument  $-\arg(z_{j+1} - z_j)$  (extending outwards to infinity). For the Helmholtz equation, let  $L_j$  denote the contour of points  $\{z \in \mathbb{C} : z = le^{-i\arg(z_{j+1} - z_j)}, l \in L_{\text{out}}\}$  (extending outwards to infinity) with  $L_{\text{out}}$  shown in Figure 8. The representations are then given as

$$(C.4) \quad u(x, y) = \frac{1}{2\pi} \sum_{j=1}^n \int_{l_j} e^{i\lambda z} \frac{\hat{u}_j(\lambda)}{\lambda} d\lambda \quad (\text{Lap.}),$$

$$(C.5) \quad u(x, y) = \frac{1}{4\pi} \sum_{j=1}^n \int_{l_j} e^{i\frac{\kappa}{2}(\lambda z - \bar{x})} \frac{\hat{u}_j(\lambda)}{\lambda} d\lambda \quad (\text{mod. Helm.}),$$

$$(C.6) \quad u(x, y) = \frac{1}{4\pi} \sum_{j=1}^n \int_{L_j} e^{i\frac{\kappa}{2}(\lambda z + \bar{x})} \frac{\hat{u}_j(\lambda)}{\lambda} d\lambda \quad (\text{Helm.}).$$

For numerical evaluation, we remark that it was proven in [29] that the integrands are bounded at the origin and decay exponentially.

**Author contributions.** The first author developed the method and its implementation and performed the numerical tests. The second and third authors assisted the first author in writing the paper.

#### REFERENCES

- [1] M. ABLOWITZ, A. FOKAS, AND Z. MUSSLIMANI, *On a new non-local formulation of water waves*, J. Fluid Mech., 562 (2006), pp. 313–343.
- [2] B. K. ALPERT AND V. ROKHLIN, *A fast algorithm for the evaluation of Legendre expansions*, SIAM J. Statist. Sci. Comput., 12 (1991), pp. 158–179.
- [3] D. AMBROSE AND D. NICHOLLS, *Fokas integral equations for three dimensional layered-media scattering*, J. Comput. Phys., 276 (2014), pp. 1–25.
- [4] T. ARENS, S. CHANDLER-WILDE, AND J. DESANTO, *On integral equation and least squares methods for scattering by diffraction gratings*, Commun. Comput. Phys., 1 (2006), pp. 1010–1042.
- [5] A. ASHTON, *On the rigorous foundations of the Fokas method for linear elliptic partial differential equations*, Proc. A, 468 (2012), pp. 1325–1331.
- [6] A. ASHTON, *Elliptic PDEs with constant coefficients on convex polyhedra via the unified method*, J. Math. Anal. Appl., 425 (2015), pp. 160–177.
- [7] A. ASHTON AND K. CROOKS, *Numerical analysis of Fokas' unified method for linear elliptic PDEs*, Appl. Numer. Math., 104 (2016), pp. 120–132.
- [8] A. ASHTON AND A. FOKAS, *A non-local formulation of rotational water waves*, J. Fluid Mech., 689 (2011), pp. 129–148.
- [9] A. ASHTON AND A. FOKAS, *Elliptic boundary value problems in convex polygons with low regularity boundary data via the unified method*, Complex Var. Elliptic Equ., 60 (2015) pp. 596–619.
- [10] I. BABUŠKA AND B. GUO, *Optimal estimates for lower and upper bounds of approximation errors in the  $p$ -version of the finite element method in two dimensions*, Numer. Math., 85 (2000), pp. 219–255.

- [11] I. BABUŠKA AND H.-S. OH, *The  $p$ -version of the finite element method for domains with corners and for infinite domains*, Numer. Methods Partial Differential Equations, 6 (1990), pp. 371–392.
- [12] A. H. BARNETT, *Evaluation of layer potentials close to the boundary for Laplace and Helmholtz problems on analytic planar domains*, SIAM J. Sci. Comput., 36 (2014), pp. A427–A451.
- [13] T. BETCKE AND L. N. TREFETHEN, *Reviving the method of particular solutions*, SIAM Rev., 47 (2005), pp. 469–491.
- [14] C. CANUTO AND A. QUARTERONI, *Approximation results for orthogonal polynomials in Sobolev spaces*, Math. Comput., 38 (1982), pp. 67–86.
- [15] M. J. COLBROOK, L. J. AYTON, AND A. S. FOKAS, *The unified transform for mixed boundary condition problems in unbounded domains*, Proc. A, 475 (2019), 20180605.
- [16] M. J. COLBROOK, N. FLYER, AND B. FORNBERG, *On the Fokas method for the solution of elliptic problems in both convex and non-convex polygonal domains*, J. Comput. Phys., 374 (2018), pp. 996–1016.
- [17] M. COSTABEL AND M. DAUGE, *Construction of corner singularities for Agmon-Douglis-Nirenberg elliptic systems*, Math. Nachr., 162 (1993), pp. 209–237.
- [18] D. CROWDY, *Fourier–Mellin transforms for circular domains*, Comput. Methods Funct. Theory, 15 (2015), pp. 655–687.
- [19] D. CROWDY, *A transform method for Laplace’s equation in multiply connected circular domains*, IMA J. Appl. Math., 80 (2015), pp. 1902–1931.
- [20] D. CROWDY AND E. LUCA, *Solving Wiener–Hopf problems without kernel factorization*, Proc. A, 470 (2014), 20140304.
- [21] C. DAVIS AND B. FORNBERG, *A spectrally accurate numerical implementation of the Fokas transform method for Helmholtz-type PDEs*, Complex Var. Elliptic Equ., 59 (2014), pp. 564–577.
- [22] P. DAVIS, *Interpolation and Approximation*, Courier Corporation, North Chelmsford, MA, 1975.
- [23] B. DECONINCK AND K. OLIVERAS, *The instability of periodic surface gravity waves*, J. Fluid Mech., 675 (2011), pp. 141–167.
- [24] B. DECONINCK AND O. TRICHTCHENKO, *Stability of periodic gravity waves in the presence of surface tension*, Eur. J. Mech. B Fluids, 46 (2014), pp. 97–108.
- [25] B. DECONINCK, T. TROGDON, AND V. VASAN, *The method of Fokas for solving linear partial differential equations*, SIAM Rev., 56 (2014), pp. 159–186.
- [26] H. EHLICH AND K. ZELLER, *Auswertung der normen von interpolationsoperatoren*, Math. Ann., 164 (1966), pp. 105–112.
- [27] A. FOKAS, *A unified transform method for solving linear and certain nonlinear PDEs*, in Proc. A, 453 (1997), pp. 1411–1443.
- [28] A. FOKAS, *On the integrability of linear and nonlinear partial differential equations*, J. Math. Phys., 41 (2000), pp. 4188–4237.
- [29] A. S. FOKAS, *A Unified Approach to Boundary Value Problems*, SIAM, Philadelphia, PA, 2008.
- [30] A. FOKAS AND S. DE LILLO, *The unified transform for linear, linearizable and integrable nonlinear partial differential equations*, Phys. Scripta, 89 (2014), 038004.
- [31] A. FOKAS, N. FLYER, S. SMITHEMAN, AND E. SPENCE, *A semi-analytical numerical method for solving evolution and elliptic partial differential equations*, J. Comput. Appl. Math., 227 (2009), pp. 59–74.
- [32] A. FOKAS AND J. LENELLS, *The Unified Transform for the Modified Helmholtz Equation in the Exterior of a Square*, preprint, arXiv:1401.2502, 2014.
- [33] B. FORNBERG AND N. FLYER, *A numerical implementation of Fokas boundary integral approach: Laplace’s equation on a polygonal domain*, in Proc. A, 467 (2011), pp. 2983–3003.
- [34] S. FULTON, A. FOKAS, AND C. XENOPHONTOS, *An analytical method for linear elliptic PDEs and its numerical implementation*, J. Comput. Appl. Math., 167 (2004), pp. 465–483.
- [35] P. HASHEMZADEH, A. FOKAS, AND S. SMITHEMAN, *A numerical technique for linear elliptic partial differential equations in polygonal domains*, in Proc. A, 471 (2015), 20140747.
- [36] N. HIGHAM, *The numerical stability of barycentric lagrange interpolation*, IMA J. Numer. Anal., 24 (2004), pp. 547–556.
- [37] A. ISERLES, *A fast and simple algorithm for the computation of Legendre coefficients*, Numer. Math., 117 (2011), pp. 529–553.
- [38] G. KARNIADAKIS AND S. SHERWIN, *Spectral/HP Element Methods for Computational Fluid Dynamics*, Oxford University Press, Oxford, UK, 2013.
- [39] R. KELLOGG, *Higher order singularities for interface problems*, in The Mathematical Foundations of the Finite Element Method with Applications to Partial Differential Equations (Proc. Sympos., Univ. Maryland, Baltimore, Md., 1972), Academic Press, New York, 1972, pp. 589–602.

- [40] Z.-C. LI AND T.-T. LU, *Singularities and treatments of elliptic boundary value problems*, Math. Comput. Model., 31 (2000), pp. 97–145.
- [41] E. LUCA AND D. CROWDY, *A transform method for the biharmonic equation in multiply connected circular domains*, IMA J. Appl. Math., 83 (2018) pp. 942–976.
- [42] E. LUCA AND S. G. LLEWELLYN S, *Stokes flow through a two-dimensional channel with a linear expansion*, Quart. J. Mech. Appl. Math., 71 (2018) pp. 441–462.
- [43] W. C. H. MCLEAN, *Strongly Elliptic Systems and Boundary Integral Equations*, Cambridge University Press, Cambridge, UK, 2000.
- [44] S. N AND B. DECONINCK, *Interface problems for dispersive equations*, Stud. Appl. Math., 134 (2015), pp. 253–275.
- [45] H. NIEDERREITER, *Random Number Generation and Quasi-Monte Carlo Methods*, SIAM, Philadelphia, PA, 1992.
- [46] K. L. OLIVERAS, V. VASAN, B. DECONINCK, AND D. HENDERSON, *Recovering the water-wave profile from pressure measurements*, SIAM J. Appl. Math., 72 (2012), pp. 897–918.
- [47] D. PATHRIA AND G. KARNADAKIS, *Spectral element methods for elliptic problems in nonsmooth domains*, J. Comput. Phys., 122 (1995), pp. 83–95.
- [48] B. PELLONI, *Advances in the study of boundary value problems for nonlinear integrable PDEs*, Nonlinearity, 28 (2015), R1.
- [49] D. POTTS, G. STEIDL, AND M. TASCHE, *Fast algorithms for discrete polynomial transforms*, Math. Comp., 67 (1998), pp. 1577–1590.
- [50] C. POZRIKIDIS, *A Practical Guide to Boundary Element Methods with the Software Library BEMLIB*, CRC Press, Boca Raton, FL, 2002.
- [51] Y. SARIDAKIS, A. SIFALAKIS, AND E. PAPADOPOULOU, *Efficient numerical solution of the generalized Dirichlet–Neumann map for linear elliptic PDEs in regular polygon domains*, J. Comput. Appl. Math., 236 (2012), pp. 2515–2528.
- [52] A. SIFALAKIS, A. FOKAS, S. FULTON, AND Y. SARIDAKIS, *The generalized Dirichlet–Neumann map for linear elliptic PDEs and its numerical implementation*, J. Comput. Appl. Math., 219 (2008), pp. 9–34.
- [53] A. SIFALAKIS, S. FULTON, E. PAPADOPOULOU, AND Y. SARIDAKIS, *Direct and iterative solution of the generalized Dirichlet–Neumann map for elliptic PDEs on square domains*, J. Comput. Appl. Math., 227 (2009), pp. 171–184.
- [54] A. SIFALAKIS, E. PAPADOPOULOU, AND Y. SARIDAKIS, *Numerical study of iterative methods for the solution of the Dirichlet–Neumann map for linear elliptic PDEs on regular polygon domains*, Int. J. Appl. Math. Comput. Sci, 4 (2007), pp. 173–178.
- [55] S. SMITHEMAN, E. SPENCE, AND A. FOKAS, *A spectral collocation method for the Laplace and modified Helmholtz equations in a convex polygon*, IMA J. Numer. Anal., 30 (2010), pp. 1184–1205.
- [56] E. SPENCE, *Boundary Value Problems for Linear Elliptic PDEs*, PhD thesis, University of Cambridge, Cambridge, UK, 2011.
- [57] E. A. SPENCE, “When all else fails, integrate by parts”: *An overview of new and old variational formulations for linear elliptic PDEs*, in Unified Transform Method for Boundary Value Problems: Applications and Advances, SIAM, Philadelphia, PA, 2014, pp. 93–159.
- [58] E. SPENCE AND A. FOKAS, *A new transform method I: Domain-dependent fundamental solutions and integral representations*, in Proc. A, 466 (2010), pp. 2259–2281.
- [59] L. N. TREFETHEN, *Approximation Theory and Approximation Practice*, SIAM, Philadelphia, PA, 2013.
- [60] T. TROGDON AND B. DECONINCK, *The solution of linear constant-coefficient evolution PDEs with periodic boundary conditions*, Appl. Anal., 91 (2012), pp. 529–544.
- [61] V. VASAN AND B. DECONINCK, *The inverse water wave problem of bathymetry detection*, J. Fluid Mech., 714 (2013), pp. 562–590.
- [62] H. WANG AND S. XIANG, *On the convergence rates of Legendre approximation*, Math. Comput., 81 (2012), pp. 861–877.
- [63] J. WILKENING AND V. VASAN, *Comparison of five methods of computing the Dirichlet–Neumann operator for the water wave problem*, Contemp. Math., 635 (2015), pp. 175–210.